

Article

Lattice Boltzmann Model for Gas Flow through Tight Porous Media with Multiple Mechanisms

Junjie Ren ^{1,2,*}, Qiao Zheng ¹, Ping Guo ² and Chunlan Zhao ¹

¹ School of Sciences, Southwest Petroleum University, Chengdu 610500, China; zhengqiaotzq@126.com (Q.Z.); your_wang1119@sina.com (C.Z.)

² State Key Laboratory of Oil and Gas Reservoir Geology and Exploitation, Southwest Petroleum University, Chengdu 610500, China; guopingswpi@vip.sina.com

* Correspondence: renjunjie1900@126.com or 201599010100@swpu.edu.cn; Tel.: +86-028-83037669

Received: 14 October 2018; Accepted: 28 January 2019; Published: 1 February 2019



Abstract: In the development of tight gas reservoirs, gas flow through porous media usually takes place deep underground with multiple mechanisms, including gas slippage and stress sensitivity of permeability and porosity. However, little work has been done to simultaneously incorporate these mechanisms in the lattice Boltzmann model for simulating gas flow through porous media. This paper presents a lattice Boltzmann model for gas flow through porous media with a consideration of these effects. The apparent permeability and porosity are calculated based on the intrinsic permeability, intrinsic porosity, permeability modulus, porosity sensitivity exponent, and pressure. Gas flow in a two-dimensional channel filled with a homogeneous porous medium is simulated to validate the present model. Simulation results reveal that gas slippage can enhance the flow rate in tight porous media, while stress sensitivity of permeability and porosity reduces the flow rate. The simulation results of gas flow in a porous medium with different mineral components show that the gas slippage and stress sensitivity of permeability and porosity not only affect the global velocity magnitude, but also have an effect on the flow field. In addition, gas flow in a porous medium with fractures is also investigated. It is found that the fractures along the pressure-gradient direction significantly enhance the total flow rate, while the fractures perpendicular to the pressure-gradient direction have little effect on the global permeability of the porous medium. For the porous medium without fractures, the gas-slippage effect is a major influence factor on the global permeability, especially under low pressure; for the porous medium with fractures, the stress-sensitivity effect plays a more important role in gas flow.

Keywords: Lattice Boltzmann method; tight porous media; multiple mechanisms; porous flow

1. Introduction

Gas flows in tight porous media have recently attracted much attention because they are widely applied in engineering fields, such as oil-gas field development, chemical processes, new energy development, and so on. The wide applications of gas flows in tight porous media also stimulate great interest in experimental and theoretical studies [1–13]. Gas flow in porous media usually involves three scales: Pore scale, representative elementary volume (REV) scale, and domain scale [14]. An REV in a porous medium is the smallest volume at which the scale characteristics of the porous flow hold, and thus the flow in a porous medium can be simulated at the REV scale without detailed information of the pore structures. Compared with pore-scale models, REV-scale models have a higher computational efficiency. Therefore, recently, many REV-scale models have been proposed in the literature, such as the Darcy model, extended Darcy models (including Brinkman-extended Darcy and Forchheimer–Darcy models), and generalized model based on the generalized Navier–Stokes equations.

Because the generalized Navier–Stokes equations [15] can consider the combined influences of the fluid and solid drag forces, they have received much attention recently. In general, these REV-scale models can be solved by the conventional numerical methods, such as the finite difference method, finite volume method, and so on [16].

The lattice Boltzmann method (LBM) is considered a promising method for simulating fluid flow and has been successfully applied to the flow in tight porous media [17–21]. According to the spatial scale in simulations, the lattice Boltzmann (LB) model for porous flow can be classified into two categories, i.e., the pore-scale LB model and REV-scale LB model, which are used to simulate the flow in porous media at the pore and REV scales, respectively. Owing to the advantage of the LBM in the simulation of fluid dynamics, some REV-scale LB models have been proposed [22–24]. However, the macroscopic equations derived from these REV-scale LB models are the Darcy equation and extended Darcy equations, which cannot consider the effects of all the fluid and solid drag forces. Guo and Zhao [14] presented a generalized REV-scale LB model for incompressible flow through porous media, which can recover the generalized Navier–Stokes equations [15] in the incompressible limit. Later, Guo and Zhao [25] extended the generalized REV-scale LB model [14] to thermal flow in porous media, which can be used to simulate both the velocity and temperature fields of the porous flow. Rong et al. [26] proposed an REV-scale LB model for axisymmetric thermal flow in porous media. Recently, Chen et al. [27] proposed a generalized REV-scale LB model with the Klinkenberg’s effect based on the model proposed by Guo and Zhao [14]. It was found that the Klinkenberg’s effect plays an important role in gas flow in tight porous media, especially when the reservoir pressure decreases.

However, in practice, gas flow through porous media in tight gas reservoirs usually takes place deep underground, where multiple mechanisms, including gas slippage and stress sensitivity of permeability and porosity, have proven to appear as the gas flows through porous media under gas-reservoir conditions [28–30]. To our knowledge, no work has been done to simultaneously incorporate these mechanisms in the LB model for simulating gas flow through porous media. Therefore, the aim of this paper is to propose an REV-scale LB model for gas flow through porous media with the consideration of these multiple mechanisms. The effects of these mechanisms on gas flow in tight porous media with (or without) fractures will be studied in detail.

2. Generalized Model for Gas Flow in Tight Porous Media

2.1. Generalized Navier–Stokes Equations

Owing to the nano/micron-sized porous media considered in the present work, the pressure difference in these porous media under gas-reservoir conditions is so small that the flow can be considered incompressible flow in simulations. Recently, the generalized Navier–Stokes equations proposed by Nithiarasu et al. [15] have been widely used to study the isothermal incompressible flow in porous media, which can be expressed as follows:

$$\nabla \cdot \mathbf{u} = 0, \quad (1a)$$

$$\partial_t \mathbf{u} + (\mathbf{u} \cdot \nabla) \left(\frac{\mathbf{u}}{\phi} \right) = -\frac{1}{\rho} \nabla p + \nu_e \nabla^2 \mathbf{u} + \mathbf{F}, \quad (1b)$$

where \mathbf{u} is the volume-averaged velocity, t is time, ϕ is the porosity, ρ is the fluid density, p is the pressure, ν_e is the effective viscosity, \mathbf{F} is the total body force, including the porous-medium resistance and other external forces expressed as follows:

$$\mathbf{F} = -\frac{\phi v}{K} \mathbf{u} - \frac{\phi F_\phi}{\sqrt{K}} |\mathbf{u}| \mathbf{u} + \phi \mathbf{G}, \quad (2)$$

where v is the shear viscosity that is not necessarily the same as ν_e , K is the permeability, \mathbf{G} is the external force, F_ϕ is the geometric function that can be expressed as [31]:

$$F_{\phi} = \frac{1.75}{\sqrt{150\phi^3}}. \quad (3)$$

Note that the pressure, p , in Equation (1b) is the fluid pressure in pores instead of the volume-averaged pressure [15]. The first and second terms on the right side of Equation (2) are the linear and nonlinear drag forces due to the presence of the porous media, respectively. Strictly speaking, the nonlinear term in Equation (2) should be considered for tight matrix and fractures. For the low-speed flow in tight matrix, the value of \mathbf{u}^2 is usually negligibly small, and thus the effect of the nonlinear drag force can be neglected for the sake of simplification, while for the high-speed flow in fractures, the nonlinear drag force should be considered owing to the large value of \mathbf{u}^2 [32,33]. In this work, the nonlinear drag force is considered for tight matrix and fractures.

2.2. Gas Slippage Effect

Owing to the small pore size in tight porous media, the Knudsen number, $\text{Kn} = \lambda/r$, where λ represents the mean free path of the gas and r is the characteristic pore size, is usually so large that the gas-slippage effect takes place and the apparent permeability increases. It should be noted that the apparent permeability reflects the real gas-transport capacity in porous media, which is dependent on the characteristics of the porous media and fluid. The initial intrinsic permeability, which only depends on the initial porous structures, is the measured liquid permeability when the pressure is the initial reservoir pressure. The relationship between the apparent permeability and initial intrinsic permeability can be given as follows:

$$K_a = K_i f_c, \quad (4)$$

where K_a is the apparent permeability, K_i is the initial intrinsic permeability, $f_c = f_p \cdot f_s$ is the total correction factor, f_p is the correction factor due to the stress-sensitivity porous structures, f_s is the correction factor due to the gas-slippage effect.

Note that the porous media are located deep underground, and thus the pore structures are sensitive to the pore pressure (or effective stress), and the permeability and porosity are functions of the pore pressure (or effective stress).

A detailed description of the stress sensitivity of permeability and porosity will be presented in the next section. Here, the stress-dependent measured liquid permeability, K_d , can be expressed as follows:

$$K_d = K_i f_p. \quad (5)$$

Note that K_d only depends on the stress-dependent porous structures, and is not affected by the fluid properties.

Similarly, the measured gas permeability without the stress sensitivity of permeability and porosity is given as follows:

$$K_s = K_i f_s, \quad (6)$$

where K_s is the Klinkenberg's corrected permeability without the effect of the stress-dependent porous structures.

To consider the influence of the gas-slippage effect, the correction factor, f_s , is introduced to correct the permeability. Currently, various expressions for f_s are proposed to describe the gas-slippage effect. Klinkenberg [29] proposed a widely used expression as follows:

$$f_s = 1 + \frac{b_k}{p}, \quad (7)$$

where b_k is the Klinkenberg's slippage factor that usually depends on the porous structures. Nevertheless, the Klinkenberg's correlation is only a first-order correlation, which may not be suitable for the tight porous media with a large Knudsen number.

Tang et al. [34] proposed a second-order correlation, which can be considered a direct extension of the Klinkenberg's correlation. The correction factor, f_s , presented by Tang et al. [34] is written as:

$$f_s = 1 + \frac{A}{p} + \frac{B}{p^2}, \quad (8)$$

where A and B are the slippage factors that depend on the mean free path, characteristic pore size, pressure, and so on.

In order to study the gas transport in all flow regimes, i.e., continuum flow ($\text{Kn} \leq 0.001$), slip flow ($0.001 < \text{Kn} \leq 0.1$), transition flow ($0.1 < \text{Kn} \leq 10$), and free molecular flow ($\text{Kn} > 10$), some scholars recommended the correction factor, f_s , as follows [35]:

$$f_s = [1 + \beta(\text{Kn})\text{Kn}] \left[1 + \frac{4\text{Kn}}{1 - b_s\text{Kn}} \right], \quad (9)$$

where b_s is the slip coefficient and is equal to -1 for slip flow, $\beta(\text{Kn})$ is the rarefaction coefficient, which is given as [36]:

$$\beta(\text{Kn}) = \frac{1.358}{1 + 0.170\text{Kn}^{-0.4348}}. \quad (10)$$

Equations (9) and (10) are derived from flows in a single pipe at micro and nano scales and have been widely applied to tight porous media. According to the definition of Kn , the mean free path, λ , and the characteristic pore size, r , should be determined to obtain the value of Kn . Based on the gas kinetic theory, the mean free path, λ , can be given by [37]:

$$\lambda = \frac{\mu}{\rho} \sqrt{\frac{\pi}{2RT}}, \quad (11)$$

where $\mu = \rho\nu$ is the dynamic viscosity, R is the gas constant, T is the temperature. Following the suggestion of Ziarani and Aguilera [38], the characteristic pore size, r , can be evaluated by [39]:

$$r = 8.886 \times 10^{-2} \left(\frac{K_d}{\phi_d} \right)^{0.5}, \quad (12)$$

where ϕ_d is the stress-dependent porosity, and the units of r and K_d are micron (μm) and millidarcy (mD), respectively.

2.3. Stress Sensitivity of Permeability and Porosity

The porous media located deep underground usually suffer from overburden pressure due to the presence of overlying rocks. In the development of oil and gas reservoirs, the pore pressure decreases as the fluid in the porous media is exploited. Therefore, the effective stress, which is approximately equal to the overburden pressure minus the pore pressure, will increase. The increase of the effective stress will result in the deformation of the reservoir rocks and then reduce the permeability and porosity. This phenomenon is called stress sensitivity of permeability and porosity. Many studies [28,30] have pointed out that these stress-sensitivity characteristics in low permeable reservoirs are especially obvious, and thus the effect of the stress sensitivity on the permeability and porosity should be considered in the simulation of gas flow in tight porous media.

The relationship between the permeability and the pore pressure is usually described by [40]:

$$K_d = K_i \exp[-\gamma(p_i - p)], \quad (13)$$

where p_i is the initial reservoir pressure, γ is the permeability modulus.

The permeability varies with the porosity, which follows the following expression [40]:

$$\frac{K_d}{K_i} = \left(\frac{\phi_d}{\phi_i} \right)^\alpha, \quad (14)$$

where α is the porosity sensitivity exponent, ϕ_i is the porosity under the initial reservoir pressure.

The pore structures in real porous media are so complex that it is difficult to obtain a generalized porosity-permeability relationship. Ergun [31] proposed an expression to describe the relationship between the permeability, K_d , and porosity, ϕ_d :

$$K_d = \frac{\phi_d^3 d_p^2}{150(1 - \phi_d)^2}, \quad (15)$$

where d_p is the solid-particle diameter. Equation (15) can be used to simulate gas flows in porous media with an approximately uniform solid-particle diameter. Note that owing to the stress sensitivity of the reservoir rocks, the solid-particle diameter, d_p , is not a constant, but a function of the pore pressure, p . However, it is difficult to determine the relationship between d_p and p , and there is little work to study this. In this work, we only use Equation (15) to approximately describe the relationship between the permeability, K_i , and porosity, ϕ_i , under the initial reservoir pressure, p_i , and the relationship between the permeability, K_d , and porosity, ϕ_d , at arbitrary reservoir pressure, p , is defined by Equation (14). The solid-particle diameter under the initial reservoir pressure is set to be d_{pi} . Therefore, in simulations, stress sensitivity could only affect the permeability and porosity, but not affect the solid-particle diameter and the structures of the porous media.

2.4. Generalized Navier–Stokes Equations for Tight Porous Media

To study gas flow through tight porous media in gas reservoirs, Equations (2) and (3) should be modified to consider the effects of the gas slippage and stress-sensitivity pore structures:

$$\mathbf{F} = -\frac{\phi_d v}{K_a} \mathbf{u} - \frac{\phi_d F_\phi}{\sqrt{K_a}} |\mathbf{u}| \mathbf{u} + \phi_d \mathbf{G}, \quad (16)$$

$$F_\phi = \frac{1.75}{\sqrt{150 \phi_d^3}}. \quad (17)$$

In summary, Equations (1), (16) and (17), together with the apparent permeability and porosity calculated by Equations (4), (9), (10), (13)–(15), compose the generalized Navier–Stokes equations for gas flow in tight porous media with multiple mechanisms.

3. Lattice Boltzmann Model

There has been considerable debate in the literature about the appropriateness of the LB model with single relaxation time for simulating Darcy flows in granular porous domains and permeability estimates [41], and the LB model with multiple relaxation times is superior to the LB model with a single relaxation time in stability and accuracy. However, the LB model with a single relaxation time has a higher computational efficiency than the LB model with multiple relaxation times and can be used to accurately simulate the porous flow at the REV scale [14,25–27]. Therefore, to simulate the gas flow in tight porous media with multiple mechanisms, we develop an LB model with a single relaxation time based on the work of Guo and Zhao [14] for gas flow through tight porous media with multiple mechanisms, which is given as follows:

$$f_i(\mathbf{r} + \mathbf{c}_i \delta_t, t + \delta_t) - f_i(\mathbf{r}, t) = -\frac{1}{\tau} \left[f_i(\mathbf{r}, t) - f_i^{(eq)}(\mathbf{r}, t) \right] + \delta_t J_i, \quad (18)$$

where:

$$f_i^{(eq)} = \omega_i \rho \left[1 + \frac{\mathbf{c}_i \cdot \mathbf{u}}{c_s^2} + \frac{(\mathbf{c}_i \cdot \mathbf{u})^2}{2\phi_d c_s^4} - \frac{\mathbf{u} \cdot \mathbf{u}}{2\phi_d c_s^2} \right], \tag{19}$$

$$J_i = \left(1 - \frac{1}{2\tau} \right) \rho \omega_i \left[\frac{\mathbf{c}_i}{c_s^2} + \frac{(\mathbf{c}_i \cdot \mathbf{u})\mathbf{c}_i - c_s^2 \mathbf{u}}{\phi_d c_s^4} \right] \cdot \mathbf{F}, \tag{20}$$

f_i is the density distribution function associated with the discrete velocity, \mathbf{c}_i , at the site, \mathbf{r} , and time t , $f_i^{(eq)}$ is the equilibrium distribution function, δ_t is the time step, τ is the dimensionless relaxation time. For the two-dimensional nine-velocity (D2Q9) model, the weight coefficients, ω_i , are $\omega_0 = 4/9$, $\omega_{1-4} = 1/9$, $\omega_{5-8} = 1/36$; $c_s = c/\sqrt{3}$ is the lattice sound speed; \mathbf{c}_i is the discrete velocity, which is given by:

$$\mathbf{c}_i = \begin{cases} (0, 0), & i = 0, \\ (\cos[(i-1)\pi/2], \sin[(i-1)\pi/2])c, & i = 1-4, \\ (\cos[(2i-9)\pi/4], \sin[(2i-9)\pi/4])\sqrt{2}c, & i = 5-8, \end{cases} \tag{21}$$

where $c = \sqrt{3RT}$.

The density and velocity are defined, respectively:

$$\rho = \sum_i f_i, \tag{22a}$$

$$\rho \mathbf{u} = \sum_i \mathbf{c}_i f_i + \frac{\delta_t}{2} \rho \mathbf{F}. \tag{22b}$$

Through the Chapman–Enskog expansion, we can derive the generalized Navier–Stokes equations presented above in the limit of a small Mach number. The pressure, p , and effective viscosity, ν_e , are defined, respectively:

$$p = \rho c_s^2, \tag{23}$$

$$\nu_e = c_s^2 \left(\tau - \frac{1}{2} \right) \delta_t. \tag{24}$$

It should be noted that \mathbf{F} includes the velocity, \mathbf{u} , and thus Equation (22b) is a nonlinear equation for the velocity, \mathbf{u} . According to the suggestion proposed by Guo and Zhao [14], the velocity, \mathbf{u} , can be obtained by:

$$\mathbf{u} = \frac{\mathbf{v}}{c_0 + \sqrt{c_0^2 + c_1 |\mathbf{v}|}}, \tag{25}$$

where \mathbf{v} is a temporal velocity given as:

$$\rho \mathbf{v} = \sum_i \mathbf{c}_i f_i + \frac{\delta_t}{2} \rho \phi_d \mathbf{G}, \tag{26}$$

and the parameters, c_0 and c_1 , are obtained by:

$$c_0 = \frac{1}{2} \left(1 + \phi_d \frac{\delta_t}{2} \frac{v}{K_a} \right), \tag{27a}$$

$$c_1 = \phi_d \frac{\delta_t}{2} \frac{F_\phi}{\sqrt{K_a}}. \tag{27b}$$

The present LB model, including Equations (18)–(27), can be used to study the gas flow in the low permeable reservoirs at the REV scale with the effects of the gas slippage and stress-sensitivity pore structures.

4. Simulation Results and Discussions

4.1. Flow in a Channel Filled with a Porous Medium

First, gas flow in a channel filled with a homogeneous porous medium is simulated to validate the present LB model. The flow is driven by pressure difference, Δp , at the inlet and outlet, which can be used to calculate the external force by $G = \Delta p / (\rho L)$ with L representing the length of the channel. The streamwise velocity, u_x (i.e., x -direction velocity), can be described by the following equation [14]:

$$\frac{v_e}{\phi_d} \frac{\partial^2 u_x}{\partial y^2} + G - \frac{v}{K_a} u_x - \frac{F_\phi}{\sqrt{K_a}} u_x^2 = 0. \quad (28)$$

with $u_x(x, 0) = u_x(x, H) = 0$, where H is the height of the channel. Owing to the extremely low velocity in tight porous media without fractures, the nonlinear inertial effect (i.e., the fourth term on the left-hand side of Equation (28)) can be neglected. Therefore, Equation (28) is simplified as:

$$\frac{v_e}{\phi_d} \frac{\partial^2 u_x}{\partial y^2} + G - \frac{v}{K_a} u_x = 0. \quad (29)$$

The analytical solution of Equation (29) is as follows:

$$u_x = \frac{GK_a}{v} \left(1 - \frac{\cosh[A(y - H/2)]}{\cosh(AH/2)} \right), \quad (30)$$

where $A = \sqrt{v\phi_d/K_a v_e}$. Note that if some fractures exist in the tight porous media, the nonlinear inertial effect needs to be considered in simulations because of the large flow rate in the fractures. In the following simulations, the effective viscosity, v_e , is assumed to equal the shear viscosity, v . The initial pressure, p_i , porosity sensitivity exponent, α , initial solid-particle diameter, d_{pi} , temperature, T , and gas constant, R , are set as 30 MPa, 3, 50 nm, 333.15 K, and 519.6545 J/(K·kg), respectively. The dynamic viscosity, μ , is calculated by the method proposed by Dempsey [42].

Figure 1 shows the effect of the permeability modulus on K_a/K_i under different pressures. It can be seen that K_a/K_i first decreases as the pressure decreases from 30 MPa, and then K_a/K_i increases as the pressure continues to decrease, which results from the combined influences of the gas slippage and stress-sensitivity pore structures. With the decrease of the pressure, the gas-slippage effect makes the permeability increase, while the stress-sensitivity effect makes the permeability decrease. The stress-sensitivity effect plays a more important role in gas transport with the increase of the permeability modulus. For a fixed value of the permeability modulus, the gas-slippage effect becomes gradually significant as the pressure decreases.

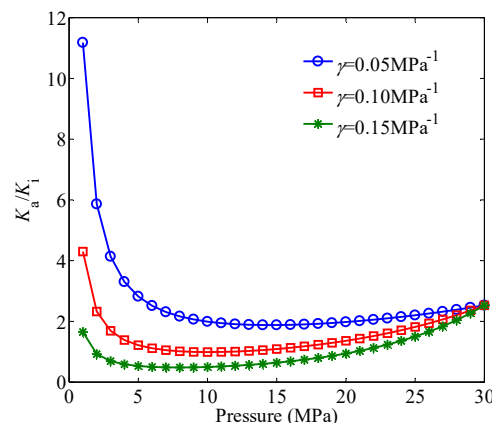


Figure 1. The effect of the permeability modulus on K_a/K_i under different pressures. The pressure varies from 1 to 30 MPa, and the initial porosity is set as $\phi_i = 0.1$.

Figure 2 shows the effect of the initial porosity on K_a/K_i under different pressures. It is clear that the gas-slippage effect becomes more obvious with the decrease of the initial porosity. For a fixed value of the initial porosity, the gas-slippage effect increases with the decrease of the pressure.

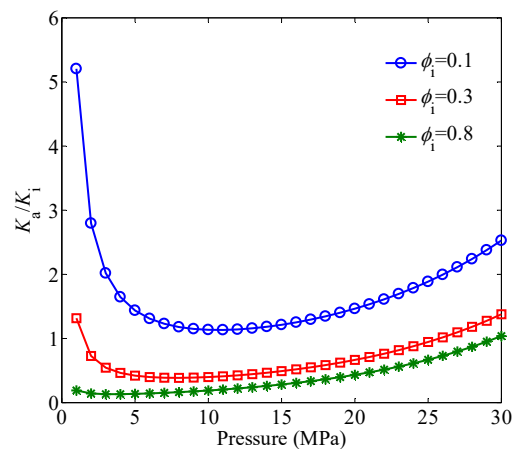


Figure 2. The effect of the initial porosity on K_a/K_i under different pressures. The pressure varies from 1 to 30 MPa, and the permeability modulus is set as $\gamma = 0.09 \text{ MPa}^{-1}$.

Figure 3 shows the effect of the permeability modulus on ϕ_d/ϕ_i under different pressures. For a given pressure, the value of ϕ_d/ϕ_i decreases with the increase of the permeability modulus. When $\gamma = 0$, the stress-sensitivity effect is neglected, and thus the porosity remains constant under different pressures. When the value of γ is small (e.g., $\gamma \leq 0.06 \text{ MPa}^{-1}$), the porosity decreases linearly as the pressure decreases. However, with the increase of the value of γ , a nonlinear relationship between the porosity and pressure will appear.

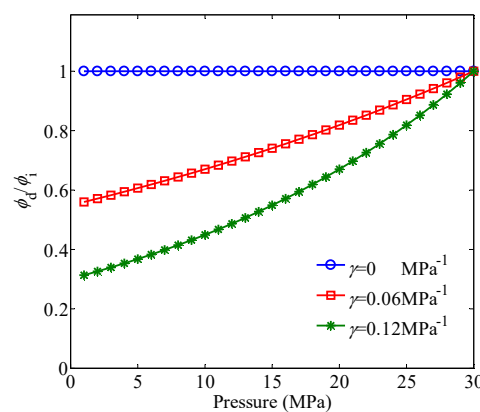


Figure 3. The effect of the permeability modulus on ϕ_d/ϕ_i under different pressures. The pressure varies from 1 to 30 MPa, and the initial porosity is set as $\phi_i = 0.1$.

In the simulations, the present LB model in lattice units is implemented, and then the simulation results are converted from lattice units to physical units [43]. Both the length and height of the channel are set as $1 \mu\text{m}$ (i.e., $L \times H = 1 \mu\text{m} \times 1 \mu\text{m}$), the initial porosity, ϕ_i , is fixed at 0.3, and the pressure gradient between the inlet and outlet is set to be 1.0 MPa/m . The lattice size is chosen as 200×200 . The dimensionless relaxation time, τ , is set as 1.0. Periodic boundary conditions are applied to the inlet and outlet, and the nonequilibrium extrapolation conditions [44] are applied to the top and bottom walls. The initial velocities (u_x and u_y) are set to be 0, and the initial density, ρ , is set as 1.0. The convergence criterion is given as follows:

$$\sqrt{\frac{\sum_{i,j} \left\{ [u_x(i,j,t+100\delta_t) - u_x(i,j,t)]^2 + [u_y(i,j,t+100\delta_t) - u_y(i,j,t)]^2 \right\}}{\sum_{i,j} [u_x(i,j,t+100\delta_t)^2 + u_y(i,j,t+100\delta_t)^2]}} < 10^{-6}. \quad (31)$$

The simulation results are shown in Figures 4 and 5, from which it is seen that the simulation results by the present LB model are in excellent agreement with the analytical solutions in all cases with different permeability moduli and pore pressures. Therefore, the present LB model has the capability to simulate gas flow through tight porous media with multiple mechanisms, including gas slippage and stress sensitivity of permeability and porosity.

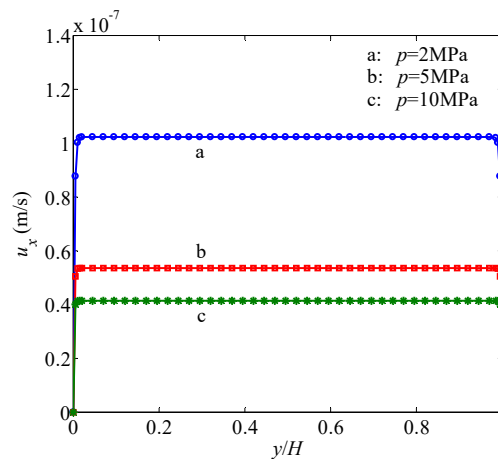


Figure 4. Velocity profiles in a channel filled with a porous medium under different pressures. Solid lines represent the analytical solutions and symbols represent the simulation results by the present model. The permeability modulus is set as $\gamma = 0.06 \text{ MPa}^{-1}$.

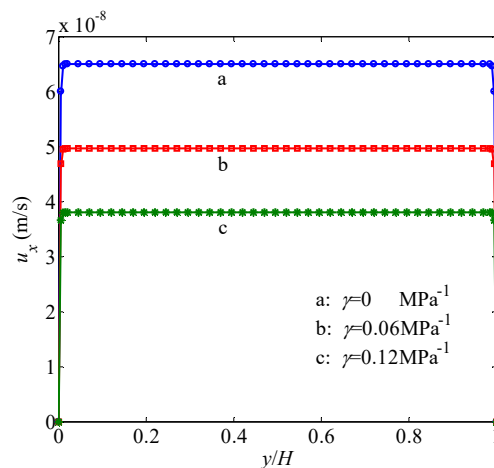


Figure 5. Velocity profiles in a channel filled with a porous medium under different permeability moduli. Solid lines represent the analytical solutions and symbols represent the simulation results by the present model. The pressure is set as $p = 25 \text{ MPa}$.

4.2. Flow in Tight Porous Media without Fractures

In practice, the real porous media are not homogeneous systems with uniform permeability and porosity, but heterogeneous systems that consist of different mineral components. Taking shale matrix as an example, shale matrix mainly consists of organic material and inorganic material. In general, the pores in shale matrix are nanoscale pores, and thus gas transport in both organic and inorganic materials is extremely slow. Compared with the inorganic material, organic material has a relatively lower permeability and porosity. Therefore, it is essential to study gas flow in porous media with

different mineral components. In this section, the structure of a heterogeneous porous medium with two mineral components is considered, which is shown in Figure 6. The randomly distributed organic material is generated by the quartet structure generation set (QSGS) method [45]. The volume fractions of the inorganic material and organic material are 0.58 and 0.42, respectively. The domain size of the porous medium is $L \times H = 2 \mu\text{m} \times 2 \mu\text{m}$. The initial porosities of inorganic material and organic material are 0.3 and 0.1, respectively. The permeability moduli of inorganic material and organic material are 0.06 MPa^{-1} and 0.12 MPa^{-1} , respectively. Periodic boundary conditions are applied to all the boundaries. The pressure gradient between the inlet and outlet is set to be 1.0 MPa/m . The dimensionless relaxation time, τ , is set as 1.0. The initial conditions and convergence criterion are the same as that in Section 4.1. The values of parameters in physical units and lattice units for simulations of gas flow in tight porous media without fractures are listed in Tables 1 and 2, respectively.

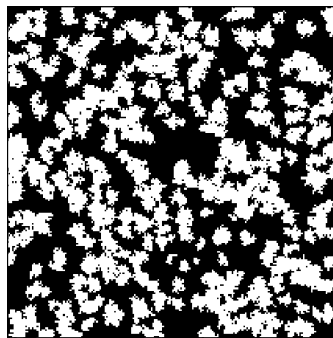


Figure 6. Structure of a heterogeneous porous medium with two mineral components: organic material with relatively lower permeability and porosity (white), and inorganic material with relatively higher permeability and porosity (black). The randomly distributed organic material is generated by the QSGS method. Volume fractions of the inorganic material and organic material are 0.58 and 0.42, respectively.

Table 1. Basic parameters in physical units used for simulations of gas flow in tight porous media without fractures.

Parameter	0.5 MPa	10 MPa	25 MPa
L (m)	2×10^{-6}	2×10^{-6}	2×10^{-6}
H (m)	2×10^{-6}	2×10^{-6}	2×10^{-6}
G ($\text{Pa} \cdot \text{m}^2/\text{kg}$)	3.4625×10^5	1.7312×10^4	6.9249×10^3
v ($\text{Pa} \cdot \text{s} \cdot \text{m}^3/\text{kg}$)	3.8651×10^{-6}	2.4740×10^{-7}	1.3805×10^{-7}
Inorganic material K_a (m^2)	4.1931×10^{-18}	5.9209×10^{-19}	9.9148×10^{-19}
Inorganic material K_d (m^2)	1.5643×10^{-19}	2.7661×10^{-19}	6.8034×10^{-19}
Inorganic material K_i (m^2)	9.1837×10^{-19}	9.1837×10^{-19}	9.1837×10^{-19}
Inorganic material ϕ_d	0.1663	0.2011	0.2715
Inorganic material ϕ_i	0.3	0.3	0.3
Organic material K_a (m^2)	1.1587×10^{-19}	1.5430×10^{-20}	3.4592×10^{-20}
Organic material K_d (m^2)	5.9698×10^{-22}	1.8666×10^{-21}	1.1292×10^{-20}
Organic material K_i (m^2)	2.0576×10^{-20}	2.0576×10^{-20}	2.0576×10^{-20}
Organic material ϕ_d	0.0307	0.0449	0.0819
Organic material ϕ_i	0.1	0.1	0.1

Table 2. Basic parameters in lattice units used for simulations of gas flow in tight porous media without fractures.

Parameter	0.5 MPa	10 MPa	25 MPa
L (lattice unit)	2	2	2
H (lattice unit)	2	2	2
G (lattice unit)	2.3178×10^{-14}	2.8284×10^{-13}	3.6310×10^{-13}
v (lattice unit)	1.0×10^{-6}	1.0×10^{-6}	1.0×10^{-6}
Inorganic material K_a (lattice unit)	4.1931×10^{-6}	5.9209×10^{-7}	9.9148×10^{-7}
Inorganic material K_d (lattice unit)	1.5643×10^{-7}	2.7661×10^{-7}	6.8034×10^{-7}

Table 2. Cont.

Parameter	0.5 MPa	10 MPa	25 MPa
Inorganic material K_i (lattice unit)	9.1837×10^{-7}	9.1837×10^{-7}	9.1837×10^{-7}
Inorganic material ϕ_d	0.1663	0.2011	0.2715
Inorganic material ϕ_i	0.3	0.3	0.3
Organic material K_a (lattice unit)	1.1587×10^{-7}	1.5430×10^{-8}	3.4592×10^{-8}
Organic material K_d (lattice unit)	5.9698×10^{-10}	1.8666×10^{-9}	1.1292×10^{-8}
Organic material K_i (lattice unit)	2.0576×10^{-8}	2.0576×10^{-8}	2.0576×10^{-8}
Organic material ϕ_d	0.0307	0.0449	0.0819
Organic material ϕ_i	0.1	0.1	0.1

The grid dependency for the simulation results is tested based on the structure of the porous medium shown in Figure 6. The two different grid sizes, namely 200×200 and, 400×400 are employed to simulate the gas flow. The effect of the grid number on the velocity magnitude distributions in the porous medium is shown in Figure 7. The velocity magnitude, $|\mathbf{u}|$, is defined as $|\mathbf{u}| = \sqrt{u_x^2 + u_y^2}$. There is no obvious difference between the velocity magnitude distributions based on the two grid system. The global permeability is introduced to quantify the seepage capability of the porous medium. Note that the global permeability defined by Chen et al. [27] is dependent on the flow field in the entire domain rather than the local characteristic of a porous medium. The definition of the global permeability is given as follows:

$$K_g = \frac{v \int_0^H |u(L, y)| dy}{H \cdot G}, \quad (32)$$

where K_g is the global permeability. It is seen from Figure 8 that no obvious change of the global permeability is observed when the grid is refined, and thus the 200×200 lattice is sufficient to obtain grid-independent results.

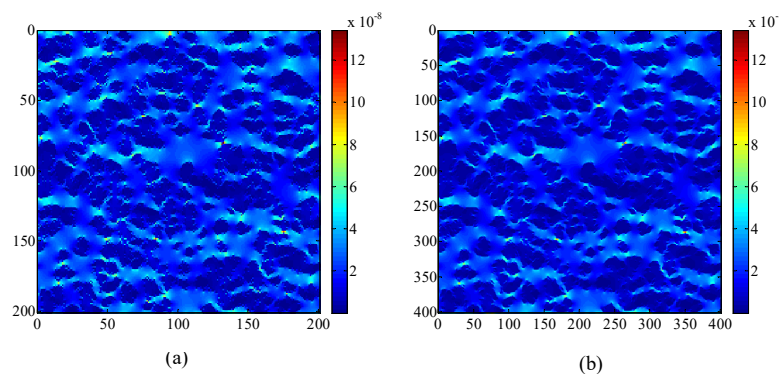


Figure 7. Velocity magnitude distributions in the porous medium based on different grid numbers. The pressure is set as $p = 10$ MPa. (a) 200×200 ; (b) 400×400 .

Figure 9 shows the effects of the gas slippage and stress-sensitivity pore structures on velocity magnitude distributions in the porous medium. The gas-slippage effect enhances the global velocity magnitude, while the stress-sensitivity effect reduces the global velocity magnitude as shown in Figure 9. It is seen that under a fixed pressure, the velocity magnitude distributions are different for the cases with and without the gas-slippage and stress-sensitivity effects, which is because these influencing factors have different effects on gas transport in different materials. Figure 10 shows the effects of the gas slippage and stress-sensitivity pore structures on the velocity magnitude profiles at the outlet of the porous medium. It is clear that the velocity magnitude profiles at the outlet are also different for the cases with and without the gas-slippage and stress-sensitivity effects. Therefore, multiple mechanisms, including gas slippage and stress sensitivity of permeability and porosity, affect not only the global velocity magnitude, but also the flow field. To obtain a correct prediction of gas flow in porous media, these mechanisms should be considered in simulations.

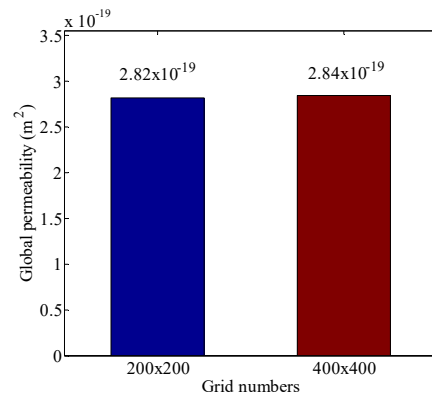


Figure 8. Global permeability based on different grid numbers. The pressure is set as $p = 10$ MPa.

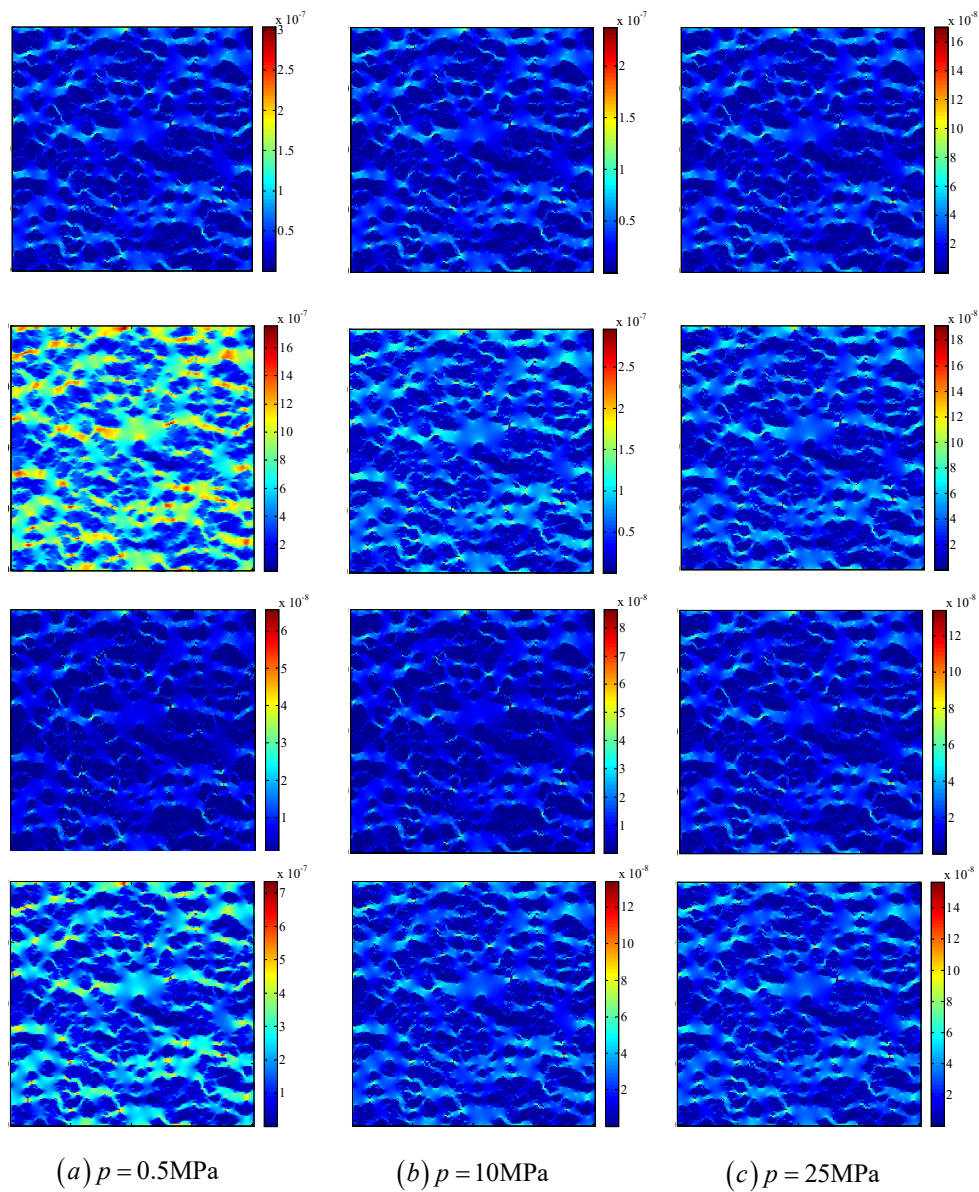


Figure 9. The effects of the gas slippage and stress-sensitivity pore structures on velocity magnitude distributions in the porous medium. (a) $p = 0.5$ MPa, (b) $p = 10$ MPa, (c) $p = 25$ MPa. The first row: without the effects of gas slippage and stress-sensitivity pore structures; the second row: with only the effect of gas slippage; the third row: with only the effect of stress-sensitivity pore structures; the fourth row: with gas slippage and stress-sensitivity pore structures.

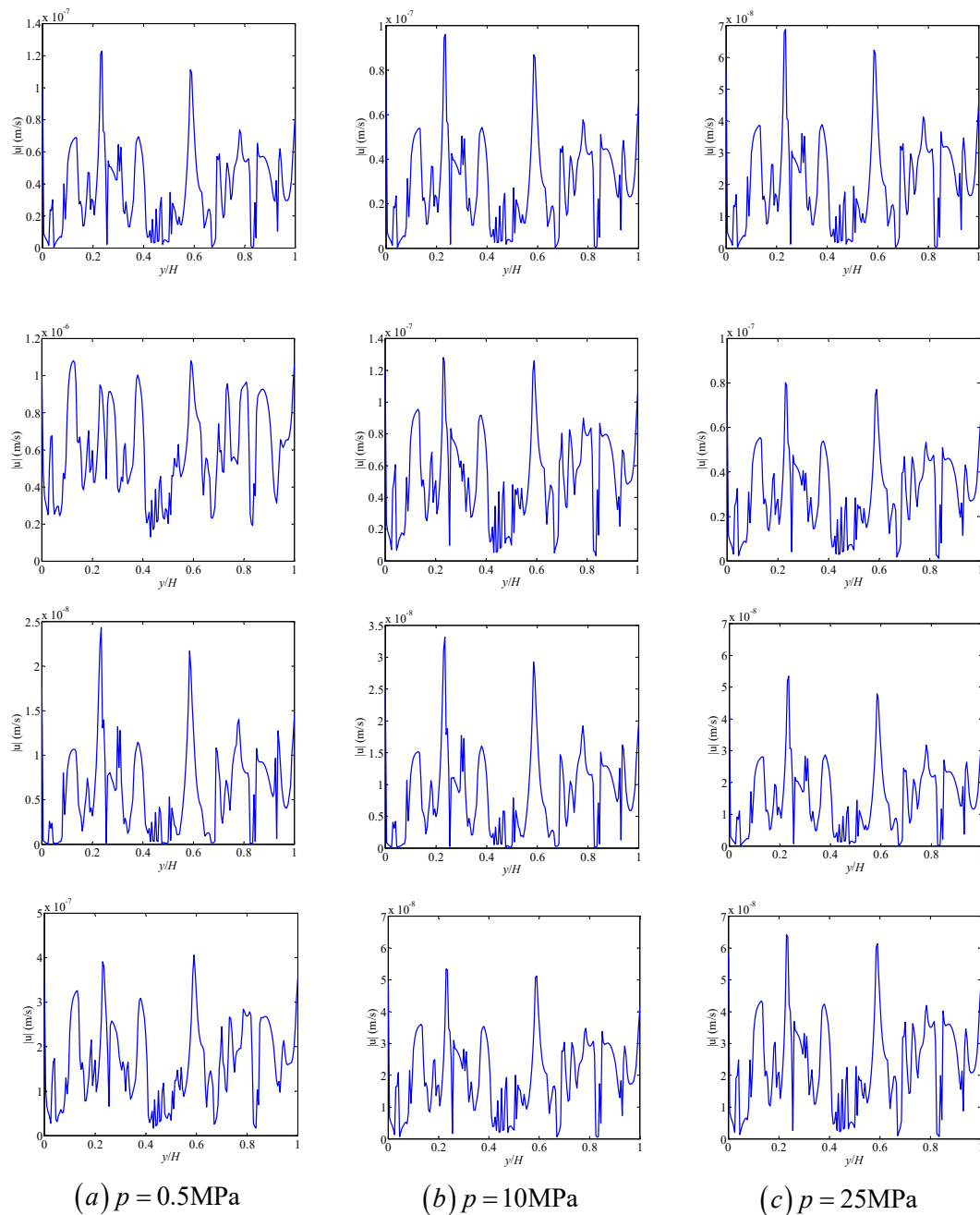


Figure 10. The effects of the gas slippage and stress-sensitivity pore structures on velocity magnitude profiles at the outlet of the porous medium. **(a)** $p = 0.5\text{ MPa}$, **(b)** $p = 10\text{ MPa}$, **(c)** $p = 25\text{ MPa}$. The first row: without the effects of gas slippage and stress-sensitivity pore structures; the second row: with only the effect of gas slippage; the third row: with only the effect of stress-sensitivity pore structures; the fourth row: with gas slippage and stress-sensitivity pore structures.

We will focus on the effects of the multiple mechanisms on the global permeability. Figure 11 shows the effects of the gas slippage and stress-sensitivity pore structures on global permeability under different pressures. It is observed that the gas slippage and stress-sensitivity pore structures significantly affect the global permeability. The gas-slippage effect increases the global permeability and becomes stronger with a decrease of the pressure. The stress-sensitivity effect decreases the global permeability as the pressure is reduced. In general, the global permeability of a porous medium deep underground is affected by the combined influences of the gas slippage and stress sensitivity. The quantitative comparison between the global permeability with and without the effects of the

gas slippage and stress-sensitivity pore structures is listed in Table 3, from which it can be seen that compared with the stress-sensitivity effect, the gas-slippage effect becomes more significant in matrix, especially under low pressure.

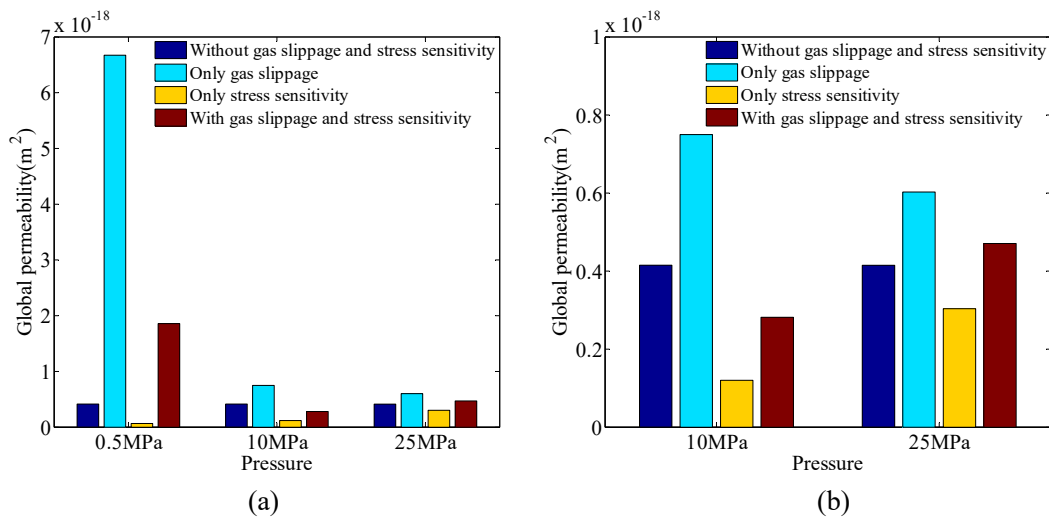


Figure 11. The effects of the gas slippage and stress-sensitivity pore structures on the global permeability under different pressures. (b) is a subfigure of (a).

Table 3. Comparison between the global permeability with and without the effects of the gas slippage and stress-sensitivity pore structures in a porous medium without fractures. The variable with the subscript, *g*, represents the corresponding global permeability.

Pressure	K_{gs}/K_{gi}	K_{gd}/K_{gi}	K_{ga}/K_{gi}
0.5 MPa	16.0734	0.1621	4.4781
10 MPa	1.8065	0.2897	0.6788
25 MPa	1.4522	0.7319	1.1345

4.3. Flow in Tight Porous Media with Fractures

In general, natural fractures may exist in a porous medium. Compared with the matrix with organic and inorganic materials, natural fractures can significantly enhance the gas-transport capability of a porous medium. In this section, gas flow in tight porous media with fractures will be studied. The effects of the fracture distributions, gas slippage, and stress sensitivity on gas transport are analyzed in detail. The distributions of the organic and inorganic materials in a porous medium are the same as that in Figure 6. The fractures with different lengths and directions are embedded in the porous medium as shown in Figure 12. The domain size of the porous medium is $20 \mu\text{m} \times 20 \mu\text{m}$, and the width of the fracture is set as $1 \mu\text{m}$. Generally, gas flow in fractures can be approximately considered as the seepage in a porous medium with extremely high porosity and permeability. The initial porosity and permeability modulus of the fractures are 0.99 and 0.03 MPa^{-1} , respectively. Periodic boundary conditions are applied to all the boundaries. The pressure gradient between the inlet and outlet is set to be 1.0 MPa/m . The dimensionless relaxation time, τ , is set as 1.0 . The initial conditions and convergence criterion are the same as that in Section 4.1. The values of parameters in physical units and lattice units for simulations of gas flow in tight porous media with fractures are listed in Table 4.

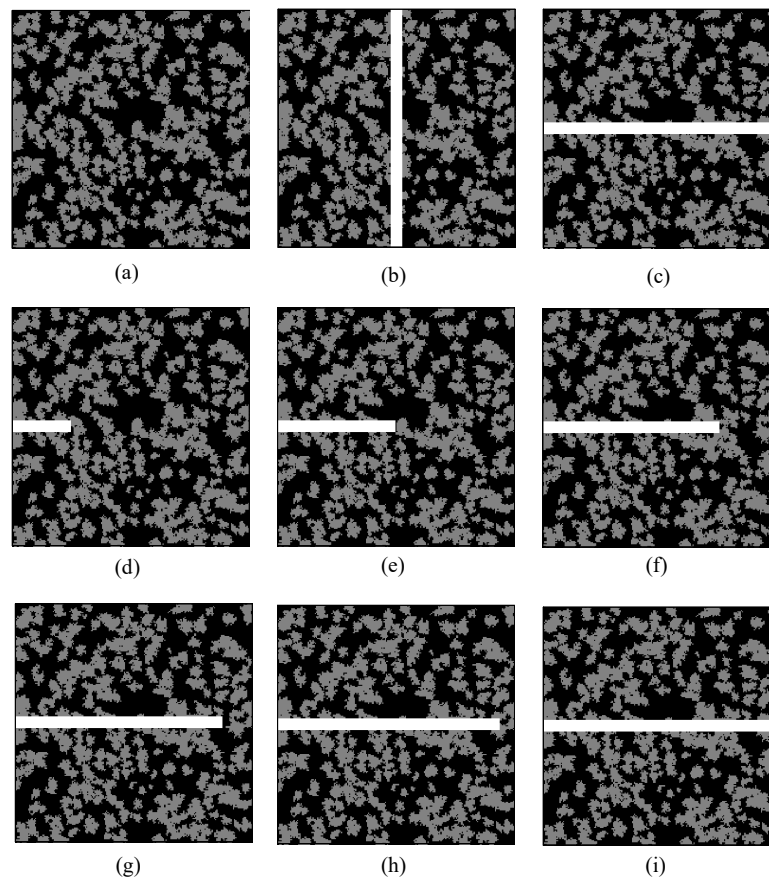


Figure 12. Structures of a heterogeneous porous medium with no fracture (a), a completely penetrated fracture along the vertical centerline (b), a completely penetrated fracture along the horizontal centerline (c), and partly penetrated fractures along the horizontal centerline with the penetration ratio being 1/4 (d), 1/2 (e), 3/4 (f), 7/8 (g), 15/16 (h), and 31/32 (i). White represents the fractures, black represents the inorganic matrix, and gray represents the organic matrix.

Table 4. Basic parameters in physical units and lattice units used for simulations of gas flow in tight porous media with fractures under the pressure of 0.5 MPa.

Parameter	Physical Unit	Lattice Unit
L	20×10^{-6} (m)	20
H	20×10^{-6} (m)	20
G	3.4625×10^5 (Pa · m ² /kg)	2.3178×10^{-14}
v	3.8651×10^{-6} (Pa · s · m ³ /kg)	1.0×10^{-6}
Inorganic material K_a	4.1931×10^{-18} (m ²)	4.1931×10^{-6}
Inorganic material K_d	1.5643×10^{-19} (m ²)	1.5643×10^{-7}
Inorganic material K_i	9.1837×10^{-19} (m ²)	9.1837×10^{-7}
Inorganic material ϕ_d	0.1663	0.1663
Inorganic material ϕ_i	0.3	0.3
Organic material K_a	1.1587×10^{-19} (m ²)	1.1587×10^{-7}
Organic material K_d	5.9698×10^{-22} (m ²)	5.9698×10^{-10}
Organic material K_i	2.0576×10^{-20} (m ²)	2.0576×10^{-8}
Organic material ϕ_d	0.0307	0.0307
Organic material ϕ_i	0.1	0.1
Natural fracture K_a	7.0996×10^{-14} (m ²)	7.0996×10^{-2}
Natural fracture K_d	6.6743×10^{-14} (m ²)	6.6743×10^{-2}
Natural fracture K_i	1.6172×10^{-13} (m ²)	1.6172×10^{-1}
Natural fracture ϕ_d	0.7371	0.7371
Natural fracture ϕ_i	0.99	0.99

Figure 13 shows the effects of the fracture distributions on velocity magnitude distributions in a porous medium. It is seen that the fracture distributions have an important effect on the flow field. When the fracture is perpendicular to the pressure-gradient direction, there is a small change of the flow field compared with a porous medium without fractures. However, when the fracture is along the pressure-gradient direction, a large change of the flow field will appear. Furthermore, the average velocity in the fracture along the pressure-gradient direction increases observably compared with that in the fracture perpendicular to the pressure-gradient direction. The average velocity in the fracture along the pressure-gradient direction increases as the length of the fracture increases. The comparison between the global permeability of a porous medium with and without fractures under the pressure of 0.5 MPa is shown in Table 5. It is observed that the fracture along the pressure-gradient direction enhances the global permeability more significantly compared with the fracture perpendicular to the pressure-gradient direction. For the fracture along the pressure-gradient direction, the penetration ratio of the fracture in the porous medium is also an important factor on the global permeability. It is found that the global permeability with completely penetrated fracture is obviously higher than that with partly penetrated fracture, and the global permeability increases when the penetration ratio increases.

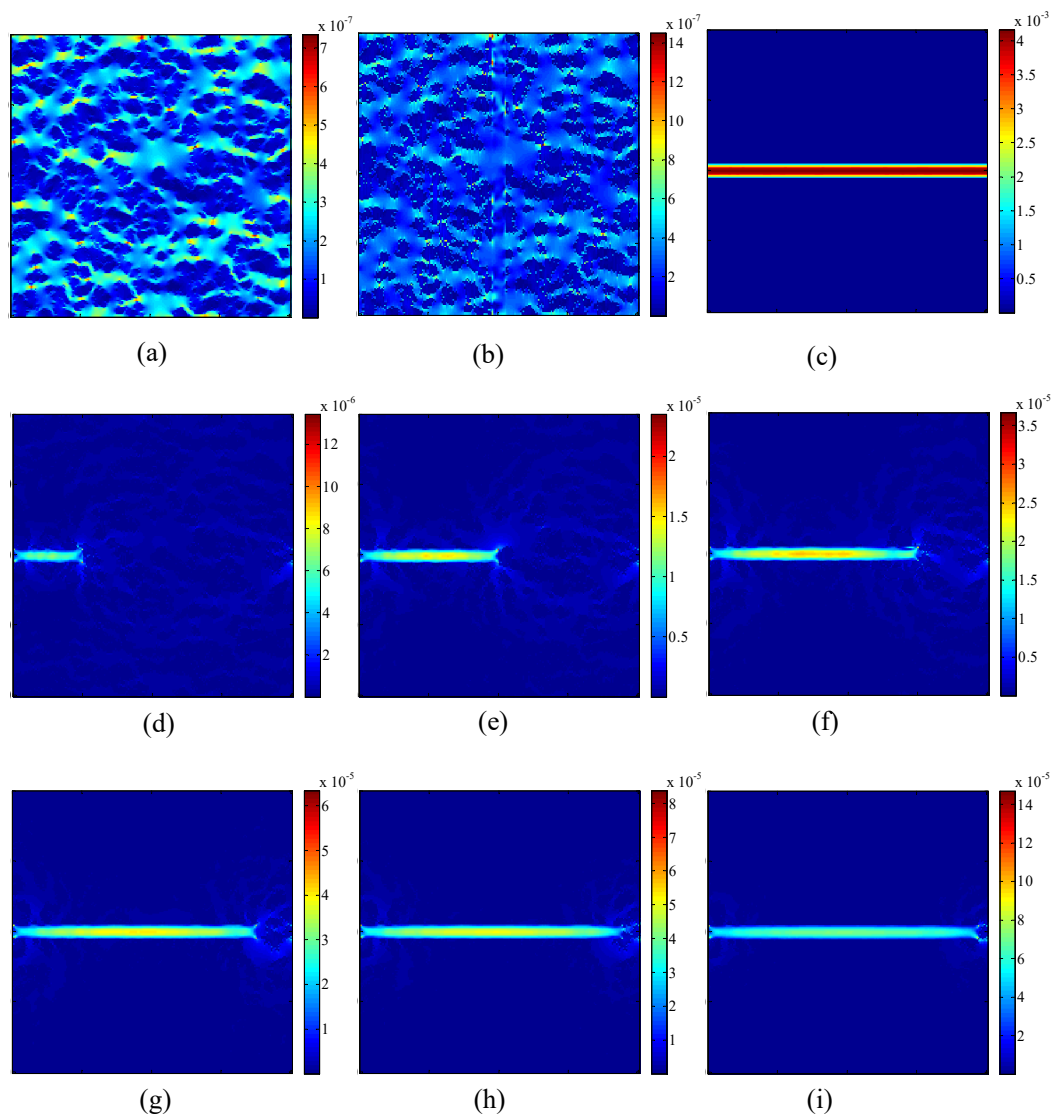


Figure 13. The effects of the fracture distributions on velocity magnitude distributions in a porous medium under the pressure of 0.5 MPa. (a–i) are the simulation results based on the structures of the porous medium shown in Figure 12a–i, respectively.

Table 5. Comparison between the global permeability of a porous medium with and without the fractures under the pressure of 0.5 MPa.

Structures of a Porous Medium with Fracture	The Ratio of Global Permeability with Fracture and Global Permeability without Fracture
Figure 12b	1.4037
Figure 12c	938.2724
Figure 12d	2.6933
Figure 12e	5.0843
Figure 12f	7.6190
Figure 12g	11.1979
Figure 12h	13.4764
Figure 12i	18.1392

The effects of the gas slippage and stress-sensitivity pore structures on global permeability of a porous medium with fractures are studied. The quantitative results are presented in Table 6, from which it is seen that the gas-slippage effect has little effect on the global permeability, while the stress-sensitivity effect significantly affects it. According to the comparison between Tables 3 and 6, it is found that for the porous medium without fractures, the gas-slippage effect is a major influence factor on the global permeability, especially under low pressure; for the porous medium with fractures, the stress-sensitivity effect plays a more important role in gas flow.

Table 6. Comparison between the global permeability with and without the effects of the gas slippage and stress-sensitivity pore structures in a porous medium with fractures. The structure of the porous medium is shown in Figure 12c. The variable with the subscript, g , represents the corresponding global permeability.

Pressure	K_{gs}/K_{gi}	K_{gd}/K_{gi}	K_{ga}/K_{gi}
0.5 MPa	1.0226	0.5594	0.5797
10 MPa	1.0014	0.6807	0.6820
25 MPa	1.0008	0.9116	0.9123

5. Conclusions

In this paper, the generalized Navier–Stokes equations were proposed for simulating gas flow through porous media with the effects of gas slippage and stress-sensitivity porous structures. The apparent permeability and porosity were obtained based on the intrinsic permeability, intrinsic porosity, permeability modulus, porosity sensitivity exponent, and pressure. An LB model was developed to solve the generalized Navier–Stokes equations. Gas flow in a two-dimensional channel filled with a homogeneous porous medium was simulated to validate the present LB model. The simulation of gas flow in a porous medium with different mineral components was carried out. The simulation results showed that the gas-slippage effect increases the global permeability of the porous medium and becomes stronger with the decrease of the pressure, while the stress-sensitivity effect decreases the global permeability as the pressure decreases. Furthermore, it was found that these effect factors affect not only the global permeability, but also the flow field. Gas flow in a porous medium with fractures was also investigated. It was found that the fractures along the pressure-gradient direction significantly enhance the total flow rate of the porous medium, while the fractures perpendicular to the pressure-gradient direction have little effect on the global permeability. For the porous medium without fractures, the gas-slippage effect is a major influence factor on the global permeability, especially under low pressure; for the porous medium with fractures, the stress-sensitivity plays a more important role in gas flow.

Author Contributions: Data curation, Q.Z.; Formal analysis, P.G.; Funding acquisition, J.R.; Investigation, J.R.; Methodology, J.R.; Project administration, J.R.; Visualization, Q.Z.; Writing—original draft, J.R.; Writing—review & editing, C.Z.

Funding: We acknowledge the support provided by Open Fund of State Key Laboratory of Oil and Gas Reservoir Geology and Exploitation (PLN201627), the Natural Science Project of Sichuan Province Department of Education (No. 17ZA0425), the Scientific Research Starting Project of SWPU (No. 2017QHZ031).

Acknowledgments: Junjie Ren would like to thank Zhaoli Guo (Huazhong University of Science and Technology) for his help.

Conflicts of Interest: The authors declare no conflict of interest.

References

- Zhang, X.; Liu, L.; Wu, Y. The Uniqueness of Positive Solution for a Fractional Order Model of Turbulent Flow in a Porous Medium. *Appl. Math. Lett.* **2014**, *37*, 26–33. [[CrossRef](#)]
- Liu, W.; Cui, J.; Xin, J. A Block-centered Finite Difference Method for an Unsteady Asymptotic Coupled Model in Fractured Media Aquifer System. *J. Comput. Appl. Math.* **2018**, *337*, 319–340. [[CrossRef](#)]
- Ren, J.; Guo, P. A Novel Semi-analytical Model for Finite-conductivity Multiple Fractured Horizontal Wells in Shale Gas Reservoirs. *J. Nat. Gas. Sci. Eng.* **2015**, *24*, 35–51. [[CrossRef](#)]
- Ren, J.; Guo, P. Anomalous Diffusion Performance of Multiple Fractured Horizontal Wells in Shale Gas Reservoirs. *J. Nat. Gas. Sci. Eng.* **2015**, *26*, 642–651. [[CrossRef](#)]
- Ren, J.; Guo, P. Performance of Vertical Fractured Wells with Multiple Finite-conductivity Fractures. *J. Geophys. Eng.* **2015**, *12*, 978–987. [[CrossRef](#)]
- Ren, J.; Guo, P. Nonlinear Flow Model of Multiple Fractured Horizontal Wells with Stimulated Reservoir Volume including the Quadratic Gradient Term. *J. Hydrol.* **2017**, *554*, 155–172. [[CrossRef](#)]
- Ren, J.; Guo, P. Nonlinear Seepage Model for Multiple Fractured Horizontal Wells with the Effect of the Quadratic Gradient Term. *J. Porous Media* **2018**, *21*, 223–239. [[CrossRef](#)]
- Ren, J.; Guo, P. A General Analytical Method for Transient Flow Rate with the Stress-sensitive Effect. *J. Hydrol.* **2018**, *565*, 262–275. [[CrossRef](#)]
- Ren, J.; Guo, P. Analytical Method for Transient Flow Rate with the Effect of the Quadratic Gradient Term. *J. Pet. Sci. Eng.* **2018**, *162*, 774–784. [[CrossRef](#)]
- Ren, J.; Guo, P.; Peng, S.; Ma, Z. Performance of Multi-stage Fractured Horizontal Wells with Stimulated Reservoir Volume in Tight Gas Reservoirs Considering Anomalous Diffusion. *Environ. Earth Sci.* **2018**, *77*, 768. [[CrossRef](#)]
- Wang, Z.; Tu, H.; Guo, P.; Zeng, F.; Sang, T.; Wang, Z. Fluid Behavior of Gas Condensate System with Water Vapor. *Fluid Phase Equilib.* **2017**, *438*, 67–75. [[CrossRef](#)]
- Wang, Z.; Li, Y.; Liu, H.; Zeng, F.; Guo, P.; Jiang, W. Study on the Adsorption, Diffusion and Permeation Selectivity of Shale Gas in Organics. *Energies* **2017**, *10*, 142. [[CrossRef](#)]
- Wang, Z.; Wang, Z.; Zeng, F.; Guo, P.; Xu, X.; Deng, D. The Material Balance Equation for Fractured Vuggy Gas Reservoirs with Bottom Water-drive Combining Stress and Gravity Effects. *J. Nat. Gas. Sci. Eng.* **2017**, *44*, 96–108. [[CrossRef](#)]
- Guo, Z.L.; Zhao, T.S. Lattice Boltzmann Model for Incompressible Flows through Porous Media. *Phys. Rev. E* **2002**, *66*, 036304. [[CrossRef](#)] [[PubMed](#)]
- Nithiarasu, P.; Seetharamu, K.N.; Sundararajan, T. Natural Convective Heat Transfer in a Fluid Saturated Variable Porosity Medium. *Int. J. Heat Mass Transf.* **1997**, *40*, 3955–3967. [[CrossRef](#)]
- Ferziger, J.H.; Perić, M. Computational Methods for Fluid Dynamics. *Phys. Today* **1997**, *50*, 80–84. [[CrossRef](#)]
- Ren, J.; Guo, P.; Guo, Z.; Wang, Z. A Lattice Boltzmann Model for simulating Gas Flow in Kerogen Pores. *Transp. Porous Med.* **2015**, *106*, 285–301. [[CrossRef](#)]
- Ren, J.; Guo, P.; Peng, S.; Yang, C. Investigation on Permeability of Shale Matrix using the Lattice Boltzmann Method. *J. Nat. Gas Sci. Eng.* **2016**, *29*, 169–175. [[CrossRef](#)]
- Ren, J.; Guo, P.; Guo, Z. Rectangular Lattice Boltzmann Equation for Gaseous Microscale Flow. *Adv. Appl. Math. Mech.* **2016**, *8*, 306–330. [[CrossRef](#)]
- Ren, J.; Guo, P. Lattice Boltzmann Simulation of Steady Flow in a Semi-Elliptical Cavity. *Commun. Comput. Phys.* **2017**, *21*, 692–717. [[CrossRef](#)]

21. Ren, J.; Zheng, Q.; Guo, P.; Peng, S.; Wang, Z.; Du, J. Pore-scale Lattice Boltzmann Simulation of Two-component Shale Gas Flow. *J. Nat. Gas. Sci. Eng.* **2019**, *61*, 46–70. [[CrossRef](#)]
22. Spaid, M.A.A.; Phelan, F.R. Lattice Boltzmann Methods for Modeling Microscale Flow in Fibrous Porous Media. *Phys. Fluids* **1997**, *9*, 2468–2474. [[CrossRef](#)]
23. Dardis, O.; McCloskey, J. Lattice Boltzmann Scheme with Real Numbered Solid Density for the Simulation of Flow in Porous Media. *Phys. Rev. E* **1998**, *57*, 4834–4837. [[CrossRef](#)]
24. Martys, N.S. Improved Approximation of the Brinkman Equation using a Lattice Boltzmann Method. *Phys. Fluids* **2001**, *13*, 1807–1810. [[CrossRef](#)]
25. Guo, Z.L.; Zhao, T.S. A Lattice Boltzmann Model for Convection Heat Transfer in Porous Media. *Numer. Heat Transf. B Fundam.* **2005**, *47*, 157–177. [[CrossRef](#)]
26. Rong, F.M.; Guo, Z.L.; Chai, Z.H.; Shi, B.C. A Lattice Boltzmann Model for Axisymmetric Thermal Flows through Porous Media. *Int. J. Heat Mass Transf.* **2010**, *53*, 5519–5527. [[CrossRef](#)]
27. Chen, L.; Fang, W.Z.; Kang, Q.J.; Hyman, J.D.; Viswanathan, H.S.; Tao, W.Q. Generalized Lattice Boltzmann Model for Flow through Tight Porous Media with Klinkenberg’s Effect. *Phys. Rev. E* **2015**, *91*, 033004. [[CrossRef](#)] [[PubMed](#)]
28. Wang, H.-X.; Wang, G.; Chen, Z.-X.; Wong, R.C.K. Deformational Characteristics of Rock in Low Permeable Reservoir and their Effect on Permeability. *J. Pet. Sci. Eng.* **2010**, *75*, 240–243. [[CrossRef](#)]
29. Klinkenberg, L.J. The Permeability of Porous Media to Liquids and Gases. *API Drill. Prod. Pract.* **1941**, *2*, 200–213. [[CrossRef](#)]
30. Vairogs, J.; Hearn, C.L.; Dareing, D.; Rhoades, V.W. Effect of Rock Stress on Gas Production from Low-permeability Reservoirs. *J. Pet. Technol.* **1971**, *23*, 1161–1167. [[CrossRef](#)]
31. Ergun, S. Fluid Flow through Packed Columns. *Chem. Eng. Prog.* **1952**, *48*, 89–94.
32. Luo, W.; Wang, X.; Feng, Y.; Tang, C.; Zhou, Y. Productivity Analysis for a Vertically Fractured Well under Non-Darcy Flow Condition. *J. Pet. Sci. Eng.* **2016**, *146*, 714–725. [[CrossRef](#)]
33. Guppy, K.H.; Cinco-Ley, H.; Ramey, H.J., Jr. Pressure Buildup Analysis of Fractured Wells Producing at High Flow Rates. *J. Pet. Technol.* **1982**, *34*, 2656–2666. [[CrossRef](#)]
34. Tang, G.H.; Tao, W.Q.; He, Y.L. Gas Slippage Effect on Microscale Porous Flow using the Lattice Boltzmann Method. *Phys. Rev. E* **2005**, *72*, 056301. [[CrossRef](#)] [[PubMed](#)]
35. Beskok, A.; Karniadakis, G.E. A Model for Flows in Channels, Pipes, and Ducts at Micro and Nano Scales. *Microsc. Therm. Eng.* **1999**, *3*, 43–77.
36. Civan, F. Effective Correlation of Apparent Gas Permeability in Tight Porous Media. *Transp. Porous Med.* **2010**, *82*, 375–384. [[CrossRef](#)]
37. Cercignani, C. *Mathematical Methods in Kinetic Theory*; Plenum Press: New York, NY, USA, 1990.
38. Ziarani, A.S.; Aguilera, R. Knudsen’s Permeability Correction for Tight Porous Media. *Transp. Porous Med.* **2012**, *91*, 239–260. [[CrossRef](#)]
39. Heid, J.G.; McMahon, J.J.; Nielsen, R.F.; Yuster, S.T. *Study of the Permeability of Rocks to Homogeneous Fluids*; American Petroleum Institute: Washington, DC, USA, 1950.
40. David, C.; Wong, T.-F.; Zhu, W.L.; Zhang, J.X. Laboratory Measurement of Compaction-induced Permeability Change in Porous Rocks: Implications for the Generation and Maintenance of Pore Pressure Excess in the Crust. *Pure Appl. Geophys.* **1994**, *143*, 425–456. [[CrossRef](#)]
41. Prestininzi, P.; Montessori, A.; La Rocca, M.; Succi, S. Reassessing the Single Relaxation Time Lattice Boltzmann Method for the Simulation of Darcy’s Flows. *Int. J. Mod. Phys. C* **2016**, *27*, 1650037. [[CrossRef](#)]
42. Dempsey, J.R. Computer Routine Treats Gas Viscosity as a Variable. *Oil Gas J.* **1965**, *63*, 141–143.
43. Succi, S. *The Lattice Boltzmann Equation for Fluid Dynamics and Beyond*; Oxford University Press: New York, NY, USA, 2001.
44. Guo, Z.L.; Zheng, C.G.; Shi, B.C. Non-equilibrium Extrapolation Method for Velocity and Boundary Conditions in the Lattice Boltzmann Method. *Chin. Phys.* **2002**, *11*, 366–374.
45. Wang, M.; Wang, J.; Pan, N.; Chen, S. Mesoscopic Predictions of the Effective Thermal Conductivity for Microscale Random Porous Media. *Phys. Rev. E* **2007**, *75*, 036702. [[CrossRef](#)] [[PubMed](#)]

